Communication

Near-Field Power Efficiency Maximization of a Bessel-Shaped Beam Through Planar Layered Media

Santi C. Pavone and Gino Sorbello

***Abstract*— We discuss the problem of power transfer maximization through locally planar layered media of focused Bessel-shaped beams (BSBs) synthesized in the near-field region, by introducing a suitable spectral figure of merit able to quantify the amount of beam power that can be efficiently delivered through an arbitrary planar multilayer structure. Such an approach is quite novel in the Fresnel region of a beam launcher since standard figures of merit normally adopted in the far-field region cannot be extended *tout court* to near-field, due to peculiar field distribution and wavefront curvature. The presented numerical results show that the adopted figure of merit can predict correctly the axicon angle for which BSBs, radiated by arrays of a given length, maximize power transmission in near-field through planar multilayer structures, and also maximize the BSB wireless power transfer efficiency.**

***Index Terms*— Bessel beams, Bessel-shaped beams (BSBs), efficiency, layered media, multilayer, near-field, wireless power transfer.**

I. Introduction

In the last decades, localized and nondiffractive waves in near-field [1], [2] deserved increasing attention both in engineering and in physics research communities [3], [4], [5], [6], [7], [8], due to their remarkable field structure and features, among which the invariance of their transverse field profile when propagating plays undoubtedly a key role. In the framework of nondiffractive waves, Bessel beams can be considered significant from both historical and technical viewpoints, since their introduction in optics by Durnin and his research group [9], [10], [11]. They represent an exact and elegant beam–wave solution of Maxwell's equations in cylindrical coordinates [12] and are theoretically not affected by diffraction and spatial spreading in free space. Despite pure Bessel beams requiring an infinite radiating distribution to be radiated, like plane waves, nowadays different high-efficiency truncated Bessel beam launchers were successfully designed and fabricated both at optical frequencies [13], [14], [15] and at microwaves and millimeter waves [16], [17], [18].

However, at present, not much attention has been paid, from an electromagnetics engineering perspective, to the propagation of Bessel beams, and, more in general, of nondiffractive waves, in more complex environments than free space (an exception can be found in [19] for the case of closed metallic cavities), such as in layered media. Recent interesting works have been devoted to the analysis, optimal design, and synthesis [20], [21], [22], [23], [24] of focusing arrays in near-field and to the maximization of wireless power transfer also in lossy media [25], [26], [27]. These general methods deserve interest, due to their remarkable potential applications in near-field communications, microwave heating, and soil disinfestation, just to mention some of them. However, the general problem of Bessel beam maximum power transfer through multilayer structures is still open and needs to be appropriately stated, not only from practical, but also from theoretical viewpoints, since standard figures of merit adopted in the far-field region, such as gain and directivity, cannot be applied in the radiative near-field region, in which nondiffractive waves are normally radiated. Hence, a suitable figure of merit for power transfer maximization needs to be properly defined [28], [29], [30].

For the sake of simplicity, in this communication an equivalent 2-D problem is stated in place of a full 3-D model since it evenly allows highlighting relevant physical phenomena, preserves beam main features (i.e., collimation, shape, focusing properties, etc.), and avoids making the formalism quite heavy to describe the canonical problem at hand. However, the achieved results are of general validity. To avoid confusion, we refer to a Bessel-shaped beam (BSB) when discussing the 2-D equivalent of Bessel beams, without loss of generality.

Therefore, in this manuscript, the problem of power transfer maximization through locally planar layered media of focused BSBs in the near-field is rigorously investigated, by defining also an appropriate figure of merit to quantify the amount of beam power that is efficiently delivered through an arbitrary planar multilayer structure. Moreover, to guarantee not only efficient power delivery beyond the stratification, but also beam focusing preservation, a constrained problem [that accounts also for the beam nondiffractive range (NDR)] is stated and solved numerically. The proposed numerical results on specific case studies pave the way to novel applications of nondiffractive waves, beyond conventional focusing in free space since a rigorous procedure is established to maximize efficiency.

The communication is structured as follows; in Section II, the formulation of both the unconstrained and constrained problems is stated, and a suitable figure of merit for BSB power transfer maximization is defined. After, in Section III, numerical results are presented for different dielectric multilayer structures, to show the effectiveness of the proposed approach. Finally, in Section IV, conclusion are drawn.

II. Problem Formulation

The equivalent 2-D geometry of the problem at hand is depicted in Fig. 1. Without loss of generality, the problem is assumed to be y-invariant, and the field is TM^z-polarized, that is, the magnetic field is oriented along the y-axis, being the extension to TE^z-polarized a simple generalization. Moreover, the standard time-harmonic convention $\exp(j\omega_0 t)$, being ω_0 the angular frequency, is assumed and suppressed throughout the communication. A BSB can be radiated by a finite electric current density distribution of the form [31]

$$\mathbf{J}(x) = J_0(k_{xa}x)\Pi\left(\frac{x}{L}\right)\hat{\mathbf{x}} \tag{1}$$

Manuscript received 28 June 2023; revised 30 January 2024; accepted 11 February 2024. Date of publication 27 February 2024; date of current version 9 April 2024. This work was supported by the European Union under the Italian National Recovery and Resilience Plan (NRRP) of NextGenerationEU, a partnership on "Telecommunications of the Future" (PE0000001–program "RESTART," Structural Project DREAMS). *(Corresponding author: Santi C. Pavone.)*

The authors are with the Department of Electrical, Electronics and Computer Engineering (DIEEI), University of Catania, 95123 Catania, Italy (e-mail: santi.pavone@unict.it).

Color versions of one or more figures in this communication are available at https://doi.org/10.1109/TAP.2024.3367411.

Digital Object Identifier 10.1109/TAP.2024.3367411

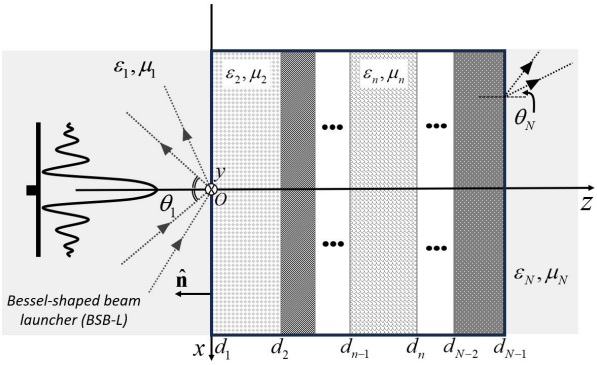

Fig. 1. Geometry of the problem. A BSB launcher (BSB-L) is used to illuminate a planar multilayer structure. Power transfer maximization is achieved by exploiting spectral wave constituents of the impinging beam.

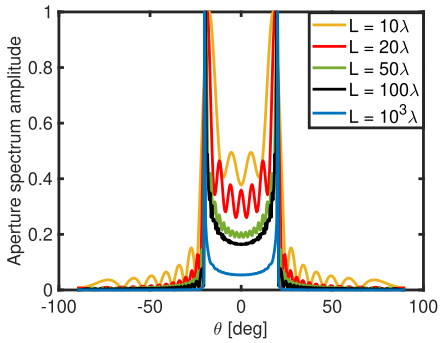

Fig. 2. Normalized angular spectrum of a BSB characterized by an axicon angle $\theta_a = 20°$, for different array lengths. As it is apparent, the spectrum is peaked in correspondence of positive and negative values of the axicon angle, due to dominant PW constituents. If aperture size increases, the amplitude spectrum tends to $\delta(\theta \mp \theta_a)$, as expected theoretically.

in which $k_{xa} = k_0 \sin\theta_a$ is the imposed wavenumber on the radiating linear distribution, $\Pi(\cdot)$ is the rectangular function, L is the array length, whereas $k_0 = \omega_0/c$ and θ_a are the free-space wavenumber and the so-called *axicon angle* of the BSB [9], [16], respectively. This latter parameter, together with the array length L, allows tuning the maximum NDR of the distribution [31], [32], that is, the maximum distance from the radiating current distribution for which the beam preserves its transverse field profile.

To evaluate the interaction of a BSB with a locally planar multilayer structure, it is interesting to determine the plane-wave (PW) spectrum of the distribution (1). Indeed, due to problem linearity, the overall response of the multilayer structure to an incoming shaped field can be written as a suitably weighted superposition of PWs. This simplifies dramatically the complexity of the problem at hand since it is reduced to the solution of a set of canonical sub-problems that can be treated separately in closed form. Thus, the PW spectrum of (1) yields

$$\begin{aligned}\tilde{\mathbf{J}}(k_x) &= \int_{-L/2}^{L/2} \mathbf{J}(x) e^{jk_x x} dx \\ &= \hat{\mathbf{x}} \int_{-L/2}^{L/2} J_0(k_{xa} x) e^{jk_x x} dx \end{aligned} \tag{2}$$

in which $k_x(\theta) = k_0 \sin\theta$ is related to the angular PW spectrum. By numerical inspection of (2) (refer to Fig. 2, in which an axicon angle $\theta_a = 20°$ is assumed as a reasonable value), it is apparent that the spectrum is peaked in correspondence of $\theta = \pm\theta_a$, that is, at the axicon angle. As a limit case, in the presence of an infinite radiating array (i.e., $L \to +\infty$), the PW amplitude spectrum is shaped as a superposition of two Dirac delta distributions at $\delta(\theta \mp \theta_a)$, that is, of two PW constituents.

This interesting result suggests that for very large current distributions like (1) ($L \gg \lambda$) radiating on a single interface between two unbounded media and under a TM^z-polarized impinging BSB, there exists a Brewster-like angle [33], [34] in which maximum transmission occurs. Thus, by matching the beam axicon angle θ_a with the theoretical Brewster angle, it is possible to achieve it. Unfortunately, such a simplistic approach applies only to simple stratifications and very large BSB launchers; it needs to be refined, by introducing a suitable figure of merit, in the presence of finite radiating current distributions, whose spectrum is still peaked but distributed also on a wide range of angles. Thus, the concept of a Brewster-like angle, despite inspiring, cannot be easily applied.

Let us focus first on the incidence of a single BSB PW constituent on the multilayer. With reference to Fig. 1, a transmission matrix (*T-matrix*) approach can be efficiently developed. By assuming $N-1$ planar interfaces between different media, it is possible to individuate $N-2$ dielectric layers. Indeed, the media labeled by $n = 1$ and $n = N$ represent the unbounded background media in front and beyond the stratification. Each dielectric layer is assumed to be linear, homogeneous, isotropic, stationary, and possibly temporally dispersive, thus characterized by electrical permittivities and magnetic permeabilities (ϵ_n, μ_n), with $n = 2, \ldots, N-1$. Moreover, the position of each interface along the z-axis is labeled by d_n, with $n = 1, \ldots, N$.

The total *T-matrix* $\bar{\mathbf{T}}^{\Sigma}$, associated with the whole stratification, can be evaluated as the product of $N-1$ matrices, associated with any planar interface, namely

$$\begin{aligned}\begin{bmatrix} T_{11}^{\Sigma} & T_{12}^{\Sigma} \\ T_{21}^{\Sigma} & T_{22}^{\Sigma} \end{bmatrix} &= \begin{bmatrix} T_{11}^{(1)} & T_{12}^{(1)} \\ T_{21}^{(1)} & T_{22}^{(1)} \end{bmatrix} \cdots \begin{bmatrix} T_{11}^{(n)} & T_{12}^{(n)} \\ T_{21}^{(n)} & T_{22}^{(n)} \end{bmatrix} \\ &\cdots \begin{bmatrix} T_{11}^{(N-1)} & T_{12}^{(N-1)} \\ T_{21}^{(N-1)} & T_{22}^{(N-1)} \end{bmatrix} = \prod_{n=1}^{N-1} \begin{bmatrix} T_{11}^{(n)} & T_{12}^{(n)} \\ T_{21}^{(n)} & T_{22}^{(n)} \end{bmatrix} \end{aligned} \tag{3}$$

in which the nth *T-matrix* relates backward $(-)$ and forward $(+)$ magnetic field complex amplitudes (i.e., H_- and H_+) at the nth interface under TM^z field polarization, namely

$$\begin{bmatrix} H_-^{(n)} \\ H_+^{(n)} \end{bmatrix} = \begin{bmatrix} T_{11}^{(n)} & T_{12}^{(n)} \\ T_{21}^{(n)} & T_{22}^{(n)} \end{bmatrix} \begin{bmatrix} H_-^{(n+1)} \\ H_+^{(n+1)} \end{bmatrix} \tag{4}$$

being

$$T_{\alpha\beta}^{(n)} = \frac{1}{2}\left[1 + (-1)^{\alpha+\beta} \frac{Z_{n+1}^{TM}}{Z_n^{TM}}\right] e^{j(-1)^{\alpha} \xi_n^{TM} d_n} e^{j(-1)^{\beta+1} \xi_{n+1}^{TM} d_n}$$

in which α and β can assume only the values 1 or 2, depending on the position of the matrix element $T_{\alpha\beta}^{(n)}$ in $\bar{\mathbf{T}}^{(n)}$; moreover, $\xi_n^{TM} = k_n \cos\theta_n$ are the propagation constants in the longitudinal direction (i.e., z-axis), $Z_n^{TM} = \eta_n \cos\theta_n$ are the equivalent TM^z impedances, $k_n = \omega_0\sqrt{\epsilon_n \mu_n}$ are the wavenumbers in each layer of the stratification, and finally $\eta_n = \sqrt{\mu_n/\epsilon_n}$ are the intrinsic impedances of each layer.

The TM^z reflection coefficient at $z = 0$ for the specific PW incidence angle θ_1, that is, $\Gamma_{TM}(\theta_1, z = 0)$, can be calculated via (3), namely

$$\begin{bmatrix} H_-^{(1)} \\ H_+^{(1)} \end{bmatrix} = \begin{bmatrix} T_{11}^{\Sigma} & T_{12}^{\Sigma} \\ T_{21}^{\Sigma} & T_{22}^{\Sigma} \end{bmatrix} \begin{bmatrix} H_-^{(N)} \\ H_+^{(N)} \end{bmatrix} = \begin{bmatrix} T_{11}^{\Sigma} & T_{12}^{\Sigma} \\ T_{21}^{\Sigma} & T_{22}^{\Sigma} \end{bmatrix} \begin{bmatrix} 0 \\ H_+^{(N)} \end{bmatrix} \tag{5}$$

by assuming as a boundary condition the fact that no reflected waves can exist in the unbounded medium N (i.e., $H_-^{(N)} = 0$). Thus, the reflection coefficient is

$$\Gamma_{TM}(\theta_1, z=0) = \frac{H_-^{(1)}(\theta_1)}{H_+^{(1)}(\theta_1)} = \frac{T_{12}^{\Sigma}(\theta_1)}{T_{22}^{\Sigma}(\theta_1)}. \tag{6}$$

The TM^z total transmission coefficient through the whole stratification, for the specific PW incidence angle θ_1, namely $\mathcal{T}_{TM}(\theta_1)$, can also be derived straightforwardly by (5) as

$$\mathcal{T}_{TM}(\theta_1) = \frac{H_+^{(N)}(\theta_1)}{H_+^{(1)}(\theta_1)} = \frac{1}{T_{22}^{\Sigma}(\theta_1)}. \tag{7}$$

It is worth noting that the calculation of $\cos\theta_n$ of nth layer requires the use of 2^{nd} Snell law, so that $\cos\theta_n = \sqrt{1-(\mu_{n-1}\epsilon_{n-1})/(\mu_n\epsilon_n)\sin^2\theta_{n-1}}$, with $n = 2, \ldots, N$.

Once the interaction (i.e., Γ_{TM}, $\mathcal{T}_{TM}$) of each BSB PW spectral constituent with the stratification is calculated for any incidence angle θ_i, the maximization of BSB power transfer through the stratification is obtained as weighted superposition of each PW transmittance and the pertinent complex spectral weight precalculated via (2). Thus, the BSB near-field power transfer η_{wpt}^{BSB} can be defined as

$$\begin{aligned}\eta_{wpt}^{BSB}(\theta_a) &= \frac{\int_{-\pi/2}^{\pi/2} |\mathcal{T}_{TM}(\theta_1)\tilde{J}(\theta_a;\theta_1)|^2 d\theta_1}{\int_{-\pi/2}^{\pi/2} |\tilde{J}(\theta_1)|^2 d\theta_1} \\ &\approx \frac{\sum_{i=1}^{N_\theta} |\mathcal{T}_{TM}(\theta_{1i})\tilde{J}(\theta_a;\theta_{1i})|^2}{\sum_{i=1}^{N_\theta} |\tilde{J}(\theta_a;\theta_{1i})|^2}\end{aligned} \tag{8}$$

being $\tilde{J}(\theta_1)$ the PW spectral weights, and N_θ the number of points used to discretize the angular range $-\pi/2 \le \theta_1 \le \pi/2$. The computational burden to evaluate (8) is negligible, since the proposed model is essentially analytical. However, to ensure accurate angular discretization, $\Delta\theta_1 = 1^\circ$ has been chosen, so that $N_\theta = 181$ points. The relation (8) is appealing, due to its simplicity and inherent physical interpretation; indeed, the overall BSB wireless power transfer through a general dielectric stratification can be thought of as the weighted superposition (via the local PW transmission coefficient $\mathcal{T}_{TM}$) of each PW constituent. Power normalization at the denominator has been introduced to make the efficiency definition independent of the specific source spectrum and to be smaller than (or equal to) one if the first and last background media are equal to each other.

At this point, a further consideration should be made, to allow the use of (8) in practical applications, in which beam focusing is required beyond the layered medium. Indeed, despite the model described above allowing prediction of the axicon angle for which the maximum amount of power is delivered through the stratification, once the dimension L of the radiating aperture has been set, no additional requirements on beam focalization beyond the layers are imposed. However, in some applications, for instance, in microwave heating, beam focusing is of primary importance. Thus, a certain range of acceptable NDR in free space can be additionally set a priori (that, in turn, bounds also the range of *feasible* axicon angles, since the current distribution length is fixed by design), so that $d_1 < \mathrm{NDR} < d_2$. In conclusion, efficiency maximization can be rewritten in terms of a constrained problem of the form

$$\begin{cases} \max\limits_{\theta_a} \quad \eta_{wpt}^{BSB}(\theta_a) \\ d_1 < \mathrm{NDR}(\theta_a, L) < d_2. \end{cases} \tag{9}$$

This problem admits, in general, a unique absolute maximum, that lies at the upper (lower) boundary of the region of feasible axicon angles θ_a if the function $\eta_{wpt}^{BSB}(\theta_a)$ is monotonically increasing (decreasing); otherwise, if the function is nonmonotonic, as normally happens when the BSB interacts with complex layered media in which multiple reflections occur, the absolute maximum can belong either to the boundaries of the feasible region, or its inner portion.

As a general theoretical remark, the choice of upper and lower constraints d_1 and d_2 in (9) should be clarified, since they represent an important degree of freedom in the optimization process. Since they are related to beam shape preservation beyond the stratification, one has to ensure that $d_1, d_2 > h + h_l$, being h the distance between the BSB launcher and the planar stratification, and h_l the whole multilayer thickness. Hence, we tacitly assume $d_2 > h + h_l$ in free space, that is, in the absence of the stratification. Moreover, small axicon angles (less than 5°) are normally difficult to achieve by planar Bessel beam launchers in the 3-D case, thus in the following we will always assume as d_1 the free-space NDR corresponding to such an angle.

In Section III, some numerical examples are presented to show the application of the proposed approach.

III. Numerical Validation

We consider here some numerical case studies of near-field wireless power transfer efficiency maximization through dielectric multilayers, on which a BSB impinges. Throughout this section, the background media in front and beyond the stratification are assumed to be free space. Moreover, nonmagnetic discontinuities ($\mu_n = \mu_0$ all over the space) are assumed, without loss of generality. Moreover, in the first two examples, the results are normalized to the operating wavelength ($\lambda = 1$ m) so that $k_0 = 2\pi$ rad/m. We also assume a large linear array of length $L = 20\lambda$ able to radiate a BSB, by synthesizing the electric current density distribution presented in (1). The axicon angle θ_a is a free design parameter to optimize in such a way as to maximize the near-field wireless power transfer efficiency of the BSB, according to the constrained optimization problem (9). The BSB launcher is assumed to be parallel to the stratification (beam normal incidence) and placed at a distance of $h = 2\lambda$ from the first interface. It is worth mentioning that the design of BSB launchers close to multilayer structures should in general consider its presence. However, if the transmittance of the layered medium is very high and the structure is matched to free space in terms of exhibited TM^z equivalent impedance over a wide angular range (let us say, larger than the axicon angle), it is possible to neglect it as a first approximation. Finally, the results in terms of field levels and maps are validated by full-wave numerical simulations by the 2-D version of COMSOL Multiphysics.

As a first example, we present a single dielectric slab in free space, characterized by an electrical permittivity $\epsilon_1 = 4\epsilon_0$, and thickness $t_1 = 1.6\lambda$. In Fig. 3(a), the plots of multilayer reflectance $|\Gamma_{TM}|^2$ and overall transmittance $|\mathcal{T}_{TM}|^2$ at the interface $z = 0$ are shown versus the incidence angle. Moreover, in Fig. 3(b), the calculation of η_{wpt}^{BSB} versus the beam axicon angle has been performed.

The allowed range of NDRs has been chosen by assuming to transmit the beam in free space beyond the dielectric stratification. This consideration allows finding a reasonable range to set a priori the constraint in (9). In the first numerical example, we assumed $d_1 \approx 6.5\lambda$ and $d_2 \gg 10\lambda$, associated with axicon angles θ_a equal to 20° and 5°, respectively.

To better show the shape of the function η_{wpt}^{BSB}, a larger range of axicon angles than the allowed region (i.e., $0^\circ < \theta_a < 40^\circ$) has been reported, whereas the forbidden range by design has been filled in yellow color. Thus, the optimal choice to maximize η_{wpt}^{BSB} is obtained for a BSB of axicon angle $\theta_a = 20^\circ$, corresponding to $\eta_{wpt}^{BSB} \approx 73\%$.

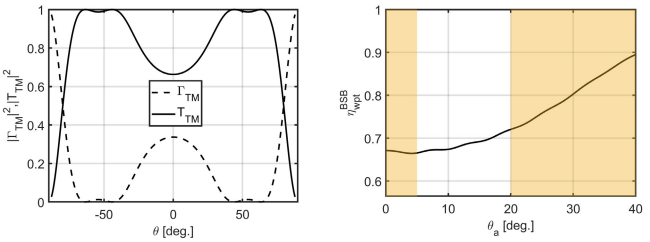

(a) (b)

Fig. 3. First example of BSB power transfer maximization through a double interface (single dielectric slab), by solving the constrained problem (9). (a) Reflectance and transmittance at the interface $z = 0$ versus plane wave incidence angle. (b) Calculation of η^{BSB}_{wpt} versus BSB axicon angle θ_a. A maximum occurs at the upper boundary of the feasible range, that is, $\eta^{BSB}_{wpt} = 73\%$ for $\theta_a = 20°$.

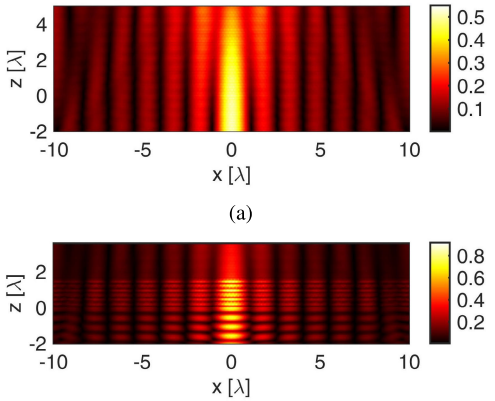

(a) (b)

Fig. 4. Nonvanishing magnetic field y-component of the optimal radiated BSB presented in the numerical example #1. Field radiated (a) free space for comparison, and (b) specific planar multilayer environment under test.

It is worth noting that the presented numerical example shows a monotonically increasing efficiency curve up to an axicon angle of 40°, so that the unconstrained optimization problem (i.e., without any limitation in the range of feasible axicon angles in such a way to guarantee not only maximum power transfer, but also beam shape preservation beyond the multilayer) allows a solution for high axicon angles. However, due to the further important requirement of beam preservation beyond the stratification, sometimes dictated by the specific application, the feasible range of axicon angles has been drastically reduced.

In Fig. 4, the nonvanishing y-component of the magnetic field radiated by the linear distribution synthesizing (1) (i.e., a BSB launcher) is shown by assuming the optimal axicon angle $\theta_a = 20°$. In particular, in Fig. 4(a), the BSB radiated in free space is reported for comparison, whereas in Fig. 4(b), the beam interaction with the stratification is highlighted. Multiple reflections and refractions occur inside the dielectric layer, and the BSB amplitude reaches values (≈ 0.8 A/m) higher than the maximum in free space (≈ 0.5 A/m), due to stationary waves inside the slab. However, beyond the stratification, the beam can preserve its focalization, as required by design.

As a second example, the interaction of a BSB with a stratification made of three different layers of electrical permittivities $(\epsilon_1, \epsilon_2, \epsilon_3) = (2, 3, 2)\epsilon_0$, and thicknesses $(t_1, t_2, t_3) = (1.8, 2.3, 0.7)\lambda$ is considered. We reported in Fig. 5(a), the magnitudes of both overall reflectance and transmittance versus each PW constituent incidence angle. Moreover, in Fig. 5(b), η^{BSB}_{wpt} has been computed versus the beam axicon angle.

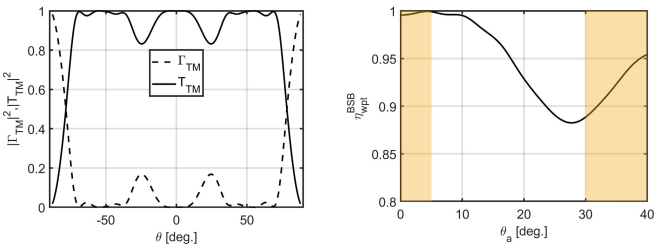

(a) (b)

Fig. 5. Second example of BSB power transfer maximization through four interfaces (symmetric triple dielectric slabs), by solving the constrained problem (9). (a) Reflectance and transmittance at the interface $z = 0$ versus plane wave incidence angle. (b) Calculation of η^{BSB}_{wpt} versus BSB axicon angle θ_a. A maximum occurs at the lower boundary of the feasible range, that is, $\eta^{BSB}_{wpt} \approx 100\%$ for $\theta_a = 5°$.

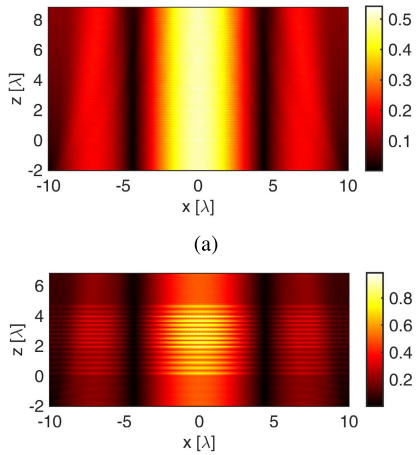

(a) (b)

Fig. 6. Nonvanishing magnetic field y-component of the optimal radiated BSB presented in the numerical example #2. Field radiated (a) free space for comparison, and (b) specific planar multilayer environment under test.

The allowed range of NDRs has been chosen by assuming, as an equivalent problem, the transmission of the beam in free space beyond the dielectric stratification. In the second numerical example, we assumed $d_1 \approx 4.5\lambda$ and $d_2 \gg 10\lambda$, associated with axicon angles θ_a equal to 30° and 5°, respectively. Also in this case, a larger range of axicon angles than the allowed region (i.e., $0° < \theta_a < 40°$) has been reported for completeness, and the forbidden range by design has been filled in yellow. The optimal axicon angle to maximize η^{BSB}_{wpt} has been achieved for $\theta_a = 5°$, corresponding to the very high value $\eta^{BSB}_{wpt} \approx 100\%$. It is worth noting that such a very large efficiency is due to the peculiar antireflective properties of the stratification. Indeed, with reference to Fig. 5(a), it can be noticed that in the neighborhood of the optimal axicon angle $\theta_a = 5°$, the transmittance is really close to 1. Since also the spectrum of the radiating distribution is dominantly peaked in the proximity of such an angle, it follows that such a stratification acts as a quasi-antireflective coating for the impinging BSB.

For the sake of clarity, in Fig. 6, the nonvanishing magnetic field y-component, radiated by the linear distribution synthesizing (1), is reported, by considering the optimal axicon angle $\theta_a = 5°$. In Fig. 6(a) the equivalent BSB radiated in free-space has been shown for comparison, whereas in Fig. 6(b) the BSB propagation inside and beyond the multilayer structure is shown. Despite multiple internal reflections and refractions within the stratification, which is more

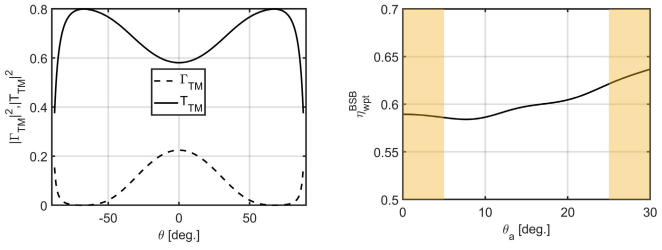

(a) (b)

Fig. 7. Third example of BSB power transfer maximization through two interfaces (i.e., a lossy slab of concrete), by solving the constrained problem (9). (a) Reflectance and transmittance at the interface $z = 0$ versus plane wave incidence angle. (b) Calculation of η_{wpt}^{BSB} versus BSB axicon angle θ_a. A maximum occurs inside the feasible range, that is, $\eta_{wpt}^{BSB} = 63\%$ for $\theta_a = 25°$.

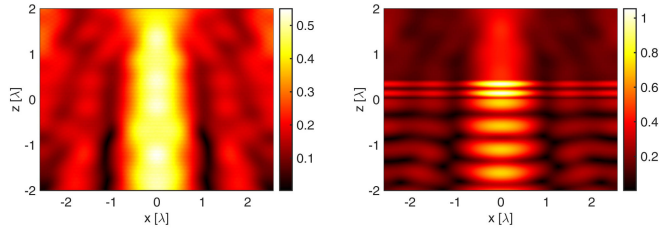

(a) (b)

Fig. 8. Non-vanishing magnetic field y-component of the optimal radiated BSB presented in the numerical example #3. Field radiated (a) free space for comparison, and (b) specific concrete slab under test.

involved than that of the first numerical example, the beam is still able to preserve its focalization, as imposed.

In the last third example, a practical situation of BSB penetration inside a layer of concrete is reported. The operating frequency has been set here to $f = 900$ MHz, so that $\lambda = 33.3$ cm, in correspondence of which the electrical permittivity is $\epsilon_1 = 6\epsilon_0$, whereas the loss tangent is $\tan\delta = 0.03$, and consequently the electrical conductivity is $\sigma = 0.003$ S/m, as shown in [35]. The thickness of concrete has been chosen to be $t_1 = 0.45\lambda \approx 15$ cm. In addition, a different radiating distribution of length $L = 4.5\lambda$ has been considered to ensure the second null of $J_0(k_{xa}x)$ falls at its boundaries for the axicon angle $\theta_a \approx 25°$. This way, beam edge-diffraction due to aperture truncation is minimized, according to the general theory of aperture antennas.

In Fig. 7(a), the magnitudes of reflection and transmission coefficients versus PW constituent incidence angle are shown, whereas in Fig. 7(b), η_{wpt}^{BSB} is calculated versus the beam axicon angle. The allowed range of NDRs has been chosen by assuming also in this case to transmit the beam in free space beyond the dielectric stratification. In this last numerical example, we assumed $d_1 \approx 4\lambda$ and $d_2 \gg 10\lambda$, associated with axicon angles θ_a equal to 25° and 5°, respectively. The optimal axicon angle to maximize η_{wpt}^{BSB} has been achieved for $\theta_a = 25°$, corresponding to an efficiency of $\eta_{wpt}^{BSB} = 63\%$. In Fig. 8, the nonvanishing magnetic field y-component has been reported, in which the optimal axicon angle $\theta_a = 25°$ has been assumed. In Fig. 8(a), the equivalent BSB radiated in free space has been presented for completeness, and in Fig. 8(b), the BSB propagation inside the planar stratification is shown. Also here, a nonnegligible stationary field pattern arises inside the dielectric layer of concrete, due to the internal reflection of some plane wave constituents inside the slab of higher permittivity than free space. However, the beam is still focused beyond the stratification, as required by design.

IV. Conclusion

In this manuscript, we dealt with the problem of power transfer maximization of focused BSBs in near-field through planar layered media, by defining a physics-based figure of merit to quantify the amount of beam power that is efficiently delivered beyond the stratification. Such an approach is quite original in the Fresnel region of a beam launcher since standard figures of merit used in the far-field region (for instance, gain and directivity) cannot be applied *tout court*, due to peculiar field distribution and wavefront curvature. In all numerical case studies, we have shown the effectiveness of the theoretical model to ensure both beam shape preservation and efficient power transmission beyond the multilayer. These results pave the way to novel applications of nondiffractive waves, beyond conventional focusing in free space, spanning from near-field communications to through-the-wall radars.

References

[1] H. E. Hernández-Figueroa, M. Zamboni-Rached, and E. Recami, *Localized Waves*, vol. 194. Hoboken, NJ, USA: Wiley, 2008.

[2] H. E. Hernández-Figueroa, M. Zamboni-Rached, and E. Recami, *Non-Diffracting Waves*. Hoboken, NJ, USA: Wiley, 2013.

[3] J.-Y. Lu and J. F. Greenleaf, "Ultrasonic nondiffracting transducer for medical imaging," *IEEE Trans. Ultrason., Ferroelectr., Freq. Control*, vol. 37, no. 5, pp. 438–447, Sep. 1990.

[4] T. A. Planchon et al., "Rapid three-dimensional isotropic imaging of living cells using Bessel beam plane illumination," *Nature Methods*, vol. 8, no. 5, pp. 417–423, May 2011.

[5] A. Mazzinghi et al., "Large depth of field pseudo-Bessel beam generation with a RLSA antenna," *IEEE Trans. Antennas Propag.*, vol. 62, no. 8, pp. 3911–3919, Aug. 2014.

[6] W. B. Williams and J. B. Pendry, "Generating Bessel beams by use of localized modes," *J. Opt. Soc. Amer. A, Opt. Image Sci.*, vol. 22, no. 5, p. 992, 2005.

[7] D. McGloin and K. Dholakia, "Bessel beams: Diffraction in a new light," *Contemp. Phys.*, vol. 46, no. 1, pp. 15–28, Jan. 2005.

[8] F. O. Fahrbach and A. Rohrbach, "Propagation stability of self-reconstructing Bessel beams enables contrast-enhanced imaging in thick media," *Nature Commun.*, vol. 3, no. 1, p. 632, Jan. 2012.

[9] J. Durnin, "Exact solutions for nondiffracting beams. I. The scalar theory," *J. Opt. Soc. Amer. A, Opt. Image Sci.*, vol. 4, no. 4, pp. 651–654, Apr. 1987.

[10] J. Durnin, J. J. Miceli, and J. H. Eberly, "Diffraction-free beams," *Phys. Rev. Lett.*, vol. 58, no. 15, pp. 1499–1501, Apr. 1987.

[11] Z. Bouchal and M. Olivík, "Non-diffractive vector Bessel beams," *J. Modern Opt.*, vol. 42, no. 8, pp. 1555–1566, Aug. 1995.

[12] A. Dudley, M. Lavery, M. Padgett, and A. Forbes, "Unraveling Bessel beams," *Opt. Photon. News*, vol. 24, no. 6, p. 22, 2013.

[13] S. Monk, J. Arlt, D. A. Robertson, J. Courtial, and M. J. Padgett, "The generation of Bessel beams at millimetre-wave frequencies by use of an axicon," *Opt. Commun.*, vol. 170, nos. 4–6, pp. 213–215, Nov. 1999.

[14] O. Brzobohatý, T. Cižmár, and P. Zemánek, "High quality quasi-Bessel beam generated by round-tip axicon," *Opt. Exp.*, vol. 16, no. 17, p. 12688, 2008.

[15] J. Arlt and K. Dholakia, "Generation of high-order Bessel beams by use of an axicon," *Opt. Commun.*, vol. 177, no. 1, pp. 297–301, Apr. 2000.

[16] S. C. Pavone, M. Ettorre, M. Casaletti, and M. Albani, "Analysis and design of Bessel beam launchers: Transverse polarization," *IEEE Trans. Antennas Propag.*, vol. 69, no. 8, pp. 5175–5180, Aug. 2021.

[17] W. Fuscaldo, G. Valerio, A. Galli, R. Sauleau, A. Grbic, and M. Ettorre, "Higher-order leaky-mode Bessel-beam launcher," *IEEE Trans. Antennas Propag.*, vol. 64, no. 3, pp. 904–913, Mar. 2016.

[18] S. Pakovic, S. Zhou, D. González-Ovejero, S. C. Pavone, A. Grbic, and M. Ettorre, "Bessel–Gauss beam launchers for wireless power transfer," *IEEE Open J. Antennas Propag.*, vol. 2, pp. 654–663, 2021.

[19] S. C. Pavone, L. Di Donato, and G. Sorbello, "Effects of a cylindrical metallic cavity on the radiation of longitudinally polarized limited-diffractive Bessel beams," *IEEE Antennas Wireless Propag. Lett.*, vol. 22, pp. 655–659, 2023.

[20] F. Tofigh, J. Nourinia, M. Azarmanesh, and K. M. Khazaei, "Near-field focused array microstrip planar antenna for medical applications," *IEEE Antennas Wireless Propag. Lett.*, vol. 13, pp. 951–954, 2014.

[21] R. Cicchetti, A. Faraone, and O. Testa, "Energy-based representation of multiport circuits and antennas suitable for near- and far-field syntheses," *IEEE Trans. Antennas Propag.*, vol. 67, no. 1, pp. 85–98, Jan. 2019.

[22] R. Cicchetti, A. Faraone, and O. Testa, "Near field synthesis based on multi-port antenna radiation matrix eigenfields," *IEEE Access*, vol. 7, pp. 62184–62197, 2019.

[23] W. Geyi, "The method of maximum power transmission efficiency for the design of antenna arrays," *IEEE Open J. Antennas Propag.*, vol. 2, pp. 412–430, 2021.

[24] F. Lisi, A. Michel, and P. Nepa, "Synthesis of near-field arrays based on electromagnetic inner products," *IEEE Trans. Antennas Propag.*, vol. 71, no. 6, pp. 4919–4931, Jun. 2023.

[25] A. Razavi, R. Maaskant, J. Yang, and M. Viberg, "Maximum aperture power transmission in lossy homogeneous matters," *IEEE Antennas Wireless Propag. Lett.*, vol. 14, pp. 175–178, 2015.

[26] K. Zhang et al., "Near-field wireless power transfer to deep-tissue implants for biomedical applications," *IEEE Trans. Antennas Propag.*, vol. 68, no. 2, pp. 1098–1106, Feb. 2020.

[27] J.-H. Kim and S. Nam, "Optimized transmitting sources for radiative wireless power transmission with lossy media," *IEEE Trans. Antennas Propag.*, vol. 70, no. 4, pp. 3106–3111, Apr. 2022.

[28] G. V. Borgiotti, "Maximum power transfer between two planar apertures in the Fresnel zone," *IEEE Trans. Antennas Propag.*, vol. AP-14, no. 2, pp. 158–163, Mar. 1966.

[29] J. D. Heebl, M. Ettorre, and A. Grbic, "Wireless links in the radiative near field via Bessel beams," *Phys. Rev. Appl.*, vol. 6, no. 3, Sep. 2016, Art. no. 034018.

[30] S. C. Pavone and M. Albani, "Design of a wireless link at microwaves in the radiative near-field by using RLSA Bessel beam launchers," in *Proc. Photon. Electromagn. Res. Symp. Spring (PIERS-Spring)*, Jun. 2019, pp. 289–294.

[31] S. C. Pavone, G. Sorbello, and L. Di Donato, "Forward and inverse scattering of metallic objects through focused Bessel-shaped fields," *IEEE Open J. Antennas Propag.*, vol. 3, pp. 911–916, 2022.

[32] S. C. Pavone, G. Sorbello, and L. Di Donato, "Improving physical optics approximation through Bessel beam scattering," *IEEE Antennas Wireless Propag. Lett.*, vol. 20, pp. 993–997, 2021.

[33] C. A. Balanis, *Advanced Engineering Electromagnetics*. Hoboken, NJ, USA: Wiley, 2012.

[34] S. J. Orfanidis, *Electromagnetic Waves and Antennas*. New Brunswick, NJ, USA: Rutgers University New Brunswick, 2002.

[35] G. Castorina, L. Di Donato, A. F. Morabito, T. Isernia, and G. Sorbello, "Analysis and design of a concrete embedded antenna for wireless monitoring applications [antenna applications corner]," *IEEE Antennas Propag. Mag.*, vol. 58, no. 6, pp. 76–93, Dec. 2016.

Open Access funding provided by 'Università degli Studi di Catania' within the CRUI CARE Agreement